Article:
Stowell, P., Fargher, S., Steer, C. et al. (1 more author) (2021) Scintillating thermal neutron detectors for cosmic ray soil moisture monitoring. Journal of Instrumentation, 16 (11). P11039.

https://doi.org/10.1088/1748-0221/16/11/p11039

Journal of Instrumentation

SISSA

PAPER • OPEN ACCESS

Scintillating thermal neutron detectors for cosmic ray soil moisture monitoring

Published by IOP Publishing for Sissa Medialab

Received: *June 15, 2021*
Revised: *September 10, 2021*
Accepted: *November 10, 2021*
Published: *November 29, 2021*

Scintillating thermal neutron detectors for cosmic ray soil moisture monitoring

P. Stowell,[a,c,*] **S. Fargher,**[b] **C. Steer**[c] **and L.F. Thompson**[b,c]

[a] *Centre for Advanced Instrumentation, Durham University, Lower Mountjoy, Durham, County Durham, U.K.*
[b] *Physics and Astronomy, University of Sheffield, Hounsfield Road, Sheffield, South Yorkshire, U.K.*
[c] *Geoptic Infrastructure Investigations Limited, Pickaxe Lane, South Warnborough, U.K.*

E-mail: john.p.stowell@durham.ac.uk

Abstract: Cosmic Ray Neutron Sensing (CRNS) is a powerful technique that allows non-invasive monitoring of soil moisture on length scales well matched for agricultural applications. One factor limiting the use of the technique within industrial agriculture settings is the high initial cost of Helium-3 or BF3 tubes typically used for ground level neutron monitoring. This paper discusses the use of Geant4 to design and optimise an alternative scintillator based epi-thermal neutron detector that may be applicable for challenges where cost is a higher driving factor than temporal resolution.

Keywords: Detector modelling and simulations I (interaction of radiation with matter, interaction of photons with matter, interaction of hadrons with matter, etc); Instrumentation for neutron sources; Neutron detectors (cold, thermal, fast neutrons); Radiation monitoring

ArXiv ePrint: 2106.06757

*Corresponding author.

https://doi.org/10.1088/1748-0221/16/11/P11039

Contents

2021 JINST 16 P11039

1 Introduction

By 2030 it is expected that, due to climate change, up to 50% of the world's population will be living in an at-risk water supply area [1]. Approximately 69% of fresh water withdrawal worldwide is for irrigation purposes [2], therefore technologies that can support smarter and more efficient irrigation practices are expected to have a large impact on global water security.

Cosmic Ray Neutron Sensing (CRNS) is a relatively new technique that could provide actionable soil moisture information for irrigation scheduling. CRNS can be deployed to monitor large sites completely non-invasively. Described in [3], the technique relies on the use of CRNS probes to continuously measure the rate of background cosmic ray neutrons back-scattered from surrounding soil. Cosmic ray induced neutrons are strongly moderated by hydrogen, therefore, an inverse correlation exists between neutron counting rate in the epithermal region (1 eV to 1 MeV kinetic energy) and local soil moisture. Typically for CRNS campaigns, Helium-3 neutron probes sensitive to thermal neutrons are used alongside HDPE moderator shields with thicknesses optimised to shift the detectors' dominant sensitivity into the epithermal region of interest [4]. In the past 10 years the CRNS technique has become a well-established method in the hydrological community that provides an effective way to measure the average soil Volumetric Water Content (VWC) over large areas [5]. Recent Monte-Carlo simulations show that the effective radial sensing footprint of a single CRNS probe is in the region of 120–230 m depending on local conditions [6]. The COSMOS-US [7] and COSMOS-U.K. [8] networks both demonstrate the suitability of the technique for long term monitoring of hydrological conditions. With more rigorous Monte-Carlo simulations of neutron transport being developed [6], the precision of the technique has increased to allow investigations

into the use of CRNS probes in more complex applications such as: deployment in built up areas [9], monitoring of canopy biomass [10], and scheduling of drip irrigation systems [11].

Adoption of managed irrigation practices is one way for countries to simultaneously reduce stress on their water resources, and build climate resilience into their water resource supply chain [12]. Whilst CRNS moisture monitoring is a powerful technique when compared to other methods that measure soil moisture over much smaller footprints, the high initial investment required for a CRNS probe is likely to limit widespread adoption of the technique by smallholder farmers. In most studies shown to date, CRNS systems have used Helium-3 detectors due to their large neutron absorption cross-section. The precision of any VWC estimate is a function of the detector's maximum cosmic ray neutron counting rate. As discussed in [13], the minimum integration time required to measure the volumetric soil moisture at the few-percent level can be reduced either by increasing the detection efficiency, e, in the signal region of interest (1 eV to 1 MeV), or increasing the effective detector volume, v. The ideal optimisation metric, M, is therefore not purely a function of the overall detector efficiency, but the combination $M = ev/c$ where c is the cost per effective volume of the system. Whilst Helium-3 provides one of the highest thermal neutron detection efficiencies available on the market, its high demand means it is not necessarily the optimal detector choice for all applications [14].

Several groups have already started looking at applying alternative technologies to Helium-3 developed in the nuclear sector in a hydrological monitoring context. Recently, Boron-lined gaseous detector systems were shown to provide counting rates significantly higher than traditional Helium-3 systems, with a modular design providing additional neutron spectral information on the incoming neutron flux [13]. Moving away from gas based systems, ^{6}LiF:ZnS based scintillator detectors are an alternative solution that can be easily scaled to build large area neutron detectors that are optimized for low counting rate applications [15]. In these systems Lithium-6 acts as a neutron capture agent, which is mixed with a high sensitivity Zinc-Sulphide scintillator to allow detection of the neutron capture products. Already several companies offer large area ^{6}LiF:ZnS neutron detectors for portal monitor applications [16, 17]. This is an application which shares many of the requirements of the CRNS technique; namely the deployment of robust, temperature stable systems in harsh outdoor environments. Recent developments of a hybrid EJ-426/EJ-420 (^{6}LiF:ZnS) and EJ-299-33 (pulse-shape discrimination plastic scintillator) detector system found it was possible to construct a mixed field radiation system sensitive to both gammas, muons, and thermal and fast neutrons [18]. This system was found to have neutron detection efficiencies of approximately 55% that of a typical Helium-3 based CRS1000 neutron detector . This presents a promising first step in developing scintillator based alternatives to Helium-3 in the CRNS agriculture sector, as there exists extensive prior work in the development and optimisation of ^{6}LiF:ZnS scintillators [19, 20], their associated trigger systems [21, 22], and correlations between muon and neutron cosmic ray intensities [23–25].

This paper assesses the feasibility of constructing low-cost neutron sensors, intended for soil moisture monitoring, out of scintillating foils made from ^{6}LiF:ZnS or BN:ZnS. In contrast to the detector shown in [18], the detectors are constructed from ^{6}LiF:ZnS foils sensitive to only the thermal component of the cosmic ray flux, and therefore their energy sensitivity is closer to that of a typical Helium-3 tube. By focusing on only the thermal neutron region they are expected to have significantly lower cost and power requirements compared to mixed neutron/gamma radiation

2021 JINST 16 P11039

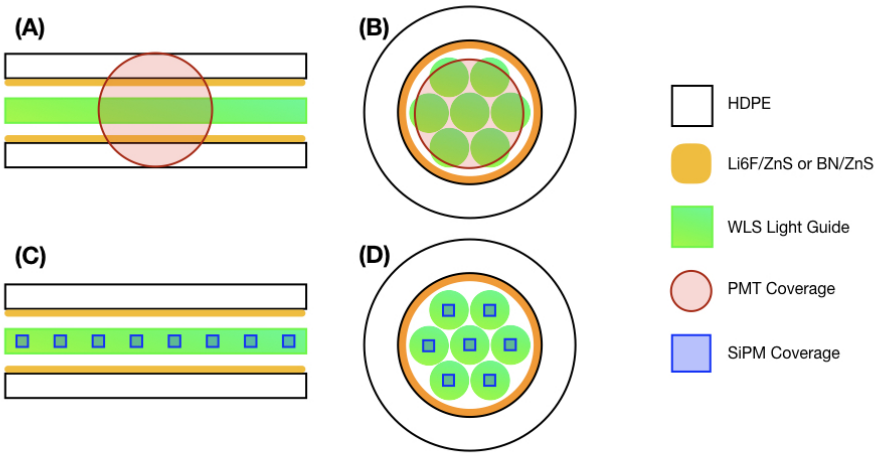

Figure 1. Comparison of possible "planar" (A and C) and "cylindrical" (B and D) detector geometries when constructing a scintillator-based neutron detector.

detectors since fast digitisers with built-in Pulse-Shape-Discrimination (PSD) are not required for efficient particle identification. Furthermore, replacing the ^{6}LiF with un-enriched BN to assess the improvement in cost versus efficiency when using readily available detector materials has been investigated through simulations to support future cost reductions of these detectors. The paper is structured as follows; section 2 describes the sensitivity of the neutron sensitive foils and the main detector design, section 3 investigates the expected detector efficiency based on GEANT4 simulations, section 4 evaluates the effect that different light guide designs have on simulated detector sensitivity, section 5 gives an overview of the detector construction and testing, section 7 provides a cost analysis of the final system, and section 8 summarises the results and future potential applications of these detectors.

2 Detector design

In neutron portal monitor applications, planar wavelength shifting neutron detector configurations have typically been used to build large area systems [17]. The use of internal reflection inside planar light guides allows large sheets of ^{6}LiF:ZnS to be optically coupled to a Photo-Multiplier Tube (PMT) with a much smaller photo-cathode area as shown in figure 1. This helps to reduce the overall cost per unit area of the system. Wavelength-shifting plastic helps to improve overall system efficiency even in the case where the emission wavelength is at a lower PMT quantum efficiency, since the likelihood of internal reflection is significantly higher if the light is emitted isotropically from within the light guide itself. Since neutron discrimination relies on detecting a train of a few photon pulses from the long ZnS decay time (of the order of 10 µs), good optical transmission is needed when constructing large planar detectors. The cost per unit area relative to traditional Helium-3 detectors is therefore dominated by the best achievable absorption length and surface quality of the light guides.

In this paper, instead of planar detectors, the efficiency of an alternative cylindrical neutron detector design, more closely resembling a traditional Helium-3 tube as shown in figure 2 is

2021 JINST 16 P11039

considered. Adopting a long cylindrical geometry in this fashion is expected to reduce the overall cost of a detection system when produced in volume. By constructing the light guides from readily available acrylic rods instead of scintillator such as EJ299-33, the detectors are expected to be predominantly sensitive to thermal neutron capture events which leads to long scintillator decay times in the ZnS. The reduction in sensitivity to gamma/muon backgrounds means thermal neutrons can easily be discriminated using the time over threshold in a low cost discriminator circuit. Furthermore, the use of cylindrical light guide assemblies allows extruded plastic to be used in place of cast PVT solutions (such as EJ280), reducing overall cost.

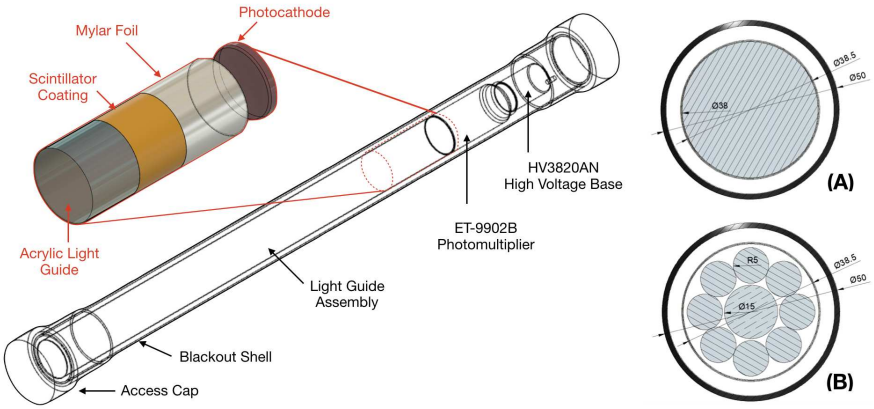

Figure 2. (left) Main cylindrical detector components. (right) The cross-section of the light guide assembly for a 38 mm cylinder (A) and segmented nine rod collection geometry (B).

The alternative detector design considered (shown in figure 2), consists of a central light guide assembly, which is wrapped in a scintillating thermal neutron foil, and coupled to an ET-Enterprises ET-9902B 38 mm diameter PMT at one end. Whilst a ET-9902B PMT has been selected for this work, the advantage of this cylindrical design is that it can be easily adapted to smaller or larger PMTs without significant internal redesign, and space-efficient outer enclosures can be constructed from light-tight tubing at low cost. Different light guide structures have been considered to assess the improvement wavelength shifting materials can make to a cylindrical detector sensitivity. In addition, the question of whether segmentation of the internal light guide can further improve the detector light yield for neutron capture events has been investigated. In [20] it was shown that fluorescent acrylic rods arranged in a grid and individually wrapped in thermal neutron scintillator could increase neutron capture light yield by up to 50% when compared to a planar light guide configuration. In this study the light guides are wrapped as one bundle by a single scintillating foil, as this allows a direct comparison of the performance of the cylindrical and segmented light guide geometries. A 38 mm diameter solid cylinder, and collections of either seven or nine smaller rods with radii chosen to optimise the coupling to a 38 mm PMT are considered as possible configurations.

3 Simulated capture efficiency

Using GEANT4 [26], the efficiency of each of the proposed thermal neutron scintillator geometries in the energy region of interest for soil moisture monitoring is evaluated. Each detector geometry is

2021 JINST 16 P11039

constructed from a 100 µm thick scintillator tube with outer diameter 38.2 mm. Scintillator material compositions are based on mixing proportions given by weight in [15, 20]. These tubes are placed around each of the simulated 50 cm long cylindrical light guide geometries. The detectors are surrounded by a moderator shield of variable thickness constructed from high density polyethylene (HDPE). In addition, a planar geometry is considered which uses the same volume of scintillator as in the cylindrical case, but instead is spread into two 5.96 cm × 50 cm sheets. These are placed either side of a 10 mm thick PVT light guide and stacked between two variable thickness layers of HDPE sheets. HDPE is assumed to have the density and composition of GEANT4's NIST material managers G4_POLYETHYLENE definition, however lower density polyethylene (LDPE) is also considered, with a density of only 0.55 g/cm^3. LDPE approximates the construction of a cylindrical moderator shield out of readily available HDPE beads with a packing fraction of 58.5%.

Neutrons are generated isotropically with a random direction from all surfaces of a 1 m radius × 2 m height cylinder surrounding the simulated detector. Random directions are used to include events in which a neutron may enter the detector at a shallow angle on the outer edge of the moderator shield, but then undergo a random scatterings and end up in the inner detector. A random starting kinetic energy between 0.01 eV and 1 GeV is chosen. This approach neglects angular assymmetries in the cosmic ray spectrum, which are expected to be significant above 10 MeV, instead deriving an approximation for the system response regardless of the deployed orientation.

The propagation of neutrons through the detector is simulated using the QGSP_BERT_HP physics model, and the total energy deposited by each neutron inside the scintillator is recorded. A neutron is assumed to have been detected if greater than 4 MeV (2 MeV) of energy is deposited in a ^{6}LiF:ZnS (BN:ZnS) layer. This neglects all effects relating to scintillator light transmission and therefore gives only an estimated capture efficiency based on the geometry of the scintillator layers and surrounding moderator. Due to the randomly chosen direction, a large proportion of neutrons miss the detector entirely. To account for this, the total neutrons detected for each geometry are divided by that predicted in a secondary simulation of a hypothetical perfect cylindrical detector (20 cm radius × 100 cm length) placed in the centre of the geometry. All efficiencies shown are relative to this hypothetical "true" detection system and therefore provide only an approximate guide on the optimal choice of moderator thickness for a generalized epithermal monitoring case. Further moderator simulation studies are required to optimize the system response on a site-by-site basis.

As shown in figure 3, the efficiency of a bare scintillator detector system is maximal at thermal neutron energies as this is where the ^{6}LiF:ZnS (BN:ZnS) capture cross-section is highest for both planar and cylindrical geometries. The GEANT4 simulations show an increased efficiency tail out to 10^6 eV for the unmoderated detector due to a small number of neutrons losing energy in the light guides before being captured. No significant differences were observed due to the slight reduction in overall detector mass when using segmented internal light guides for the cylindrical detectors, therefore comparison of the results are neglected here.

To have an optimal sensitivity in the region of interest for soil moisture monitoring both cylindrical and planar light guide geometries require an additional external neutron moderator. As shown in figure 3, the cosmic ray neutron energy spectrum at sea-level peaks in the thermal (0.01–0.1 eV) and evaporation (0.1–10 MeV) regions. However, thermal neutrons are known to carry less information on the surrounding soil moisture content across a site as they are sensitive to local changes in humidity and surface water. Similarly, approximately 10–20% of the evaporation

2021 JINST 16 P11039

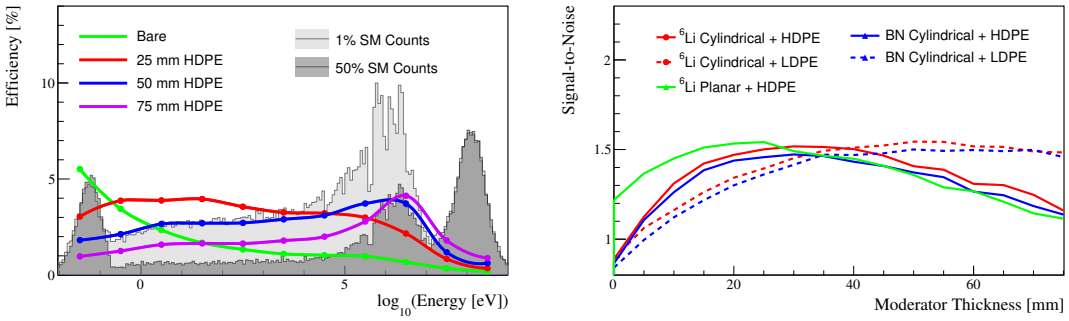

Figure 3. Capture efficiency of the different detector geometries considered in this work. (left) Capture efficiency of a cylindrical ^{6}LiF:ZnS detector as a function of starting neutron kinetic energy with varying thicknesses of HDPE moderator. The region of interest for soil moisture monitoring is shown in the shape of the light gray count histograms. (right) Calculated signal-to-noise as a function of HDPE/LDPE thickness for the different detector geometries and neutron capture agents considered in this work.

neutrons measured at ground level are from direct incoming cosmic ray neutrons with no information on local soil composition. As a result, the maximal signal to noise ratio is typically given when the signal efficiency of incoming neutrons is maximised in the 1 eV-1 MeV region whilst minimising background in both the thermal 0.01 eV-1 eV region and fast 1–1000 MeV regions. To optimise the choice of moderator thickness in each of the simulated detectors a signal-to-noise metric is used. The signal is defined as the expected difference in counts for dry and wet conditions (1% versus 50% soil moisture) after accounting for the detector efficiency as a function of energy. Similarly the background is defined as the number of counts expected for a 50% soil moisture condition. Both of the counting rate spectra were obtained by simulating 1×10^6 neutrons using the URANOS neutron simulation software with an assumed soil porosity of 50%, humidity of 1.0 g/cm^3, atmospheric depth 1020 g/cm^2, and rigidity of 10 GV.

This definition of the background is only an approximation as even at 50% soil moisture some portion of the detected neutrons carry information on local soil moisture. However, it provides a simplistic way to estimate the expected counts from the non-varying thermal and fast neutron components which both need to be minimised to maximise detector sensitivity. Thermal neutron-absorbing materials such as cadmium have been suggested as a way to suppress the thermal counts and improve signal to noise [27], however since no cadmium shields were available for long term testing in this work, this is neglected here.

Simulations of different moderator thicknesses suggest an optimal HDPE thickness of 25 mm for the planar systems and 30 mm for the cylindrical systems. This thickness of moderator is consistent with similar studies performed for Helium-3 based neutron detectors in [4]. The reduction in required moderator thickness for the planar geometry is due to an increase in average moderator thickness at the corners of the planar system. This results in 40-60% more moderator by volume compared the cylindrical case. In addition, improved signal-to-noise is observed for the planar case at low moderator thicknesses as the PVT internal light guide acts as an additional moderating shield for higher energy neutrons.

It is observed that LDPE moderator shields are also suitable for a cylindrical detector provided

2021 JINST 16 P11039

larger thicknesses of 50 mm can be used. However, using LDPE also results in a slightly higher thermal detection efficiency. The advantage of using LDPE is that a moderator shield can be constructed entirely from easily available 3 mm HDPE beads, allowing rapid modification of the moderator choice for a specific application without requiring separately cast outer HDPE shields. Future iterations of this detector will investigate the combination of HDPE beads and boron lined outer shells to produce a low cost and non-toxic optimal moderator solution. Whilst the peak signal-to-noise was found using 50 mm LDPE, comparable efficiencies to the HDPE case were found with as little as 30 mm of LDPE.

When considering the optimal moderator choice both cylindrical and planar detector geometries show a comparable efficiency when using the same volume of scintillator in each one. Whilst the total surface area of the front face of the planar detector is over 50% larger than the cylindrical detector, the efficiency averaged over all angles is similar due to the thin cross-section of the planar detector on one side. Multiple planar detectors placed at varying angles in a field could take advantage of this angular effect to extract variations in the neutron rate as a function of direction. However, doing so with a high precision would likely require much larger detectors and a higher resolution soil sampling campaign to calibrate for their varying footprints in the field. In agreement with studies shown in [20], competitive sensitivities are obtained for the un-enriched BN:ZnS detector systems when compared to ^{6}LiF:ZnS. This confirms the suitability of the material in production of low-cost neutron detectors provided scintillator detectors can be manufactured with high enough sensitivity to account for the lower scintillation light yield of BN:ZnS.

Whilst promising, the presented efficiency comparisons for planar and cylindrical detectors assume a 100% triggering efficiency once a neutron captures in the foils. In the next section the optimal light collection system for a cylindrical detector is evaluated in order to understand the maximum length of detector that could be constructed.

4 Light guide simulations

Simulations of scintillator emission for ^{6}LiF:ZnS and BN:ZnS composites and a range of light guide materials using GEANT4's optical tracking capability were performed to understand the effect light guide geometry has on overall light collection efficiency. A modification of the QGSP_BERT_HP physics list was made to include Cerenkov and scintillation light production and wavelength shifting. Optical boundaries were added to the cylindrical detector geometries discussed in the previous section using the RealSurface dynamic look-up-table, modelling the scintillator surface as a ground-to-air border, and the light guide surface as a polished-to-air border. Absorption and emission curves for each material were included as look-up tables digitized from supplier sources (figure 4). Full details of material properties included in the GEANT4 simulation are shown in table 1.

As shown in figure 4, ZnS scintillator emits in the 400 nm to 430 nm region. The 9902B photo-multiplier tube selected for this work has a sensitive region which peaks in the 430 nm region and so is well-matched for direct detection of the ZnS scintillator. It also has a width which extends out to 300-600 nm at half maximum, covering the wavelength shifting emission spectrum of EJ280 at a lower quantum efficiency. The transmission efficiency of different un-doped clear acrylics can have very different transmission curves in the high-UV region, however these differences are reduced at wavelengths greater than 400 nm so are not expected to have a significant effect on detector

2021 JINST 16 P11039

Table 1. Geant4 material definitions used in this work.

Material	R Index	Max. Absorption Length	Emission Yield	Peak Emission
^{6}LiF:ZnS	2.36	0.15 mm	47000 photons/MeV	440 nm
BN:ZnS	2.36	0.15 mm	47000 photons/MeV	440 nm
EJ280	1.58	3.50 m	-	490 nm
Clear PMMA	1.49	3.10 m	-	-
Flourescent PMMA	1.49	57.56 cm	-	550 nm

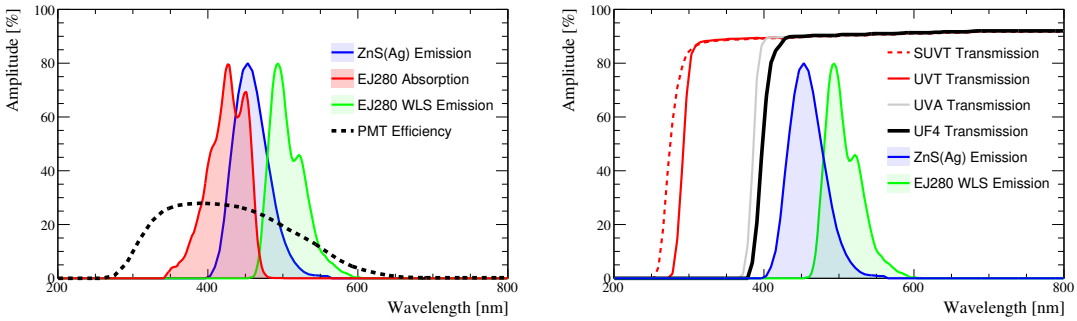

Figure 4. (left) Emission Spectrum of EJ280, ZnS and PMT efficiency. (right) Transmission properties of materials under consideration in this work.

performance. In addition to EJ280 and the available clear PMMA material, an additional material referred to simply as "Fluorescent" which is based on commercially available fluorescent rods was also considered. In [20], it was shown that off-the-shelf fluorescent rods performed substantially better than dip-coated wavelength shifting rods when trying to produce a detector 50-60 cm long. To verify this, a small quantity of fluorescent rods was acquired from a local supplier. Using a Flame-NIR-VIS spectrometer and 400 nm UV LED to test the emission spectrum of these rods, it was observed that the spectrum is shifted slightly towards the yellow, peaking at approximately 550 nm as shown in figure 5. Similar results were seen in [20] which were hypothesised to be a result of a larger proportion of fluorescence doping compared to EJ280 which leads to a higher probability of re-absorption of emitted photons in the 450-500 nm region. The absorption length of these fluorescent rods when considering the relative change in overall light transmission for all wavelengths for different distances was determined to be 57.56 ± 5.68 cm.

Simulations of light yield are performed by generating a logarithmic energy distribution of neutrons in the same way as described in section 3, and directing them at the cylindrical detector geometries, now with a full description of scintillator emission and optical tracking throughout the detector included. For each event the total number of photons detected at the PMT placed at one end of the light guide is recorded alongside the location of the true energy deposit position inside the scintillator layer. The PMT quantum efficiency distribution is accounted for by randomly throwing away photons at the simulation analysis stage based on the arriving photon wavelength. The number of remaining photons is then used to build a map of the reduction in light collected as a function of neutron capture distance along the light guide. Since the scintillator is assumed to be a

2021 JINST 16 P11039

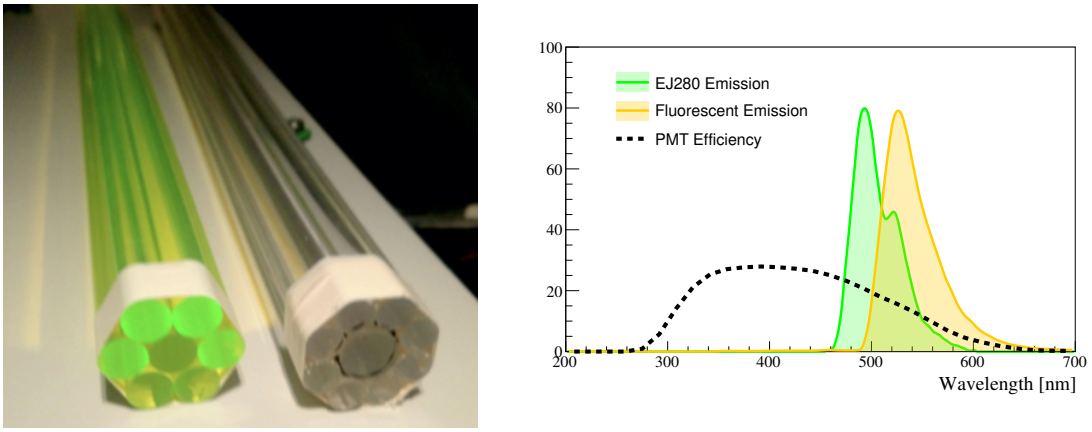

Figure 5. (left) Two different light guide geometries considered and difference between fluorescent and undoped acrylic. (right) Difference in emission spectrum for commercially available fluorescent rods and EJ280.

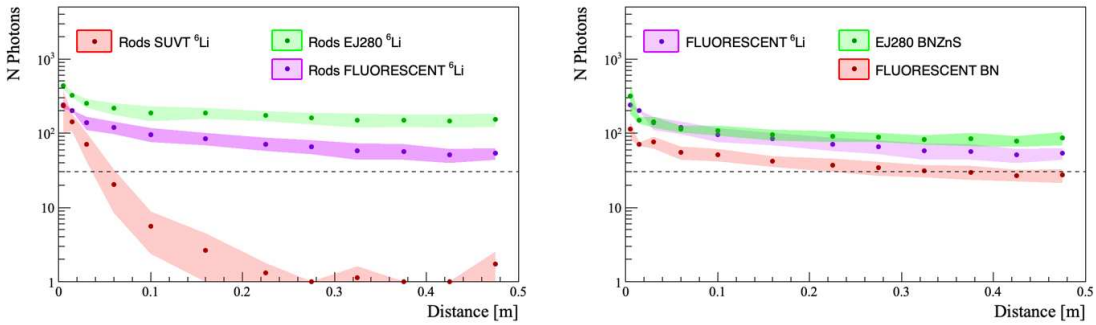

Figure 6. Number of emitted photons as a function of distance for different light guide geometries and construction materials. Bands correspond to the spread in detected photons per event as a function of the neutron capture position. The dashed line gives a guide for a 30 photon cut-off. (left) Comparison of light intensity fall-off for different light guide materials. (right) Comparison of light intensity for both ^{6}LiF:ZnS and BN:ZnS scintillator assemblies.

homogeneous solution of ^{6}LiF:ZnS (BN:ZnS) these maps do not include any variations in sensitivity due to microscopic variations in the scintillator (for example due to choice of Zn or Li^{6}F/BN grain size, or variations in scintillator thickness across the detector).

As expected, a reduction in the number of photons detected with increasing distance is observed. Most notable however is the large excess of photons within 5-10 cm of the PMT face which are a result of photons emitted from the scintillator travelling directly into the PMT without being captured in the light guide. In the case of clear acrylic light guides, capture inside the acrylic is minimal, since any scintillation photons created at an angle suitable for total internal reflection have a high probability of reflecting off the exterior of the acrylic light guide back towards the opaque scintillator coating. To estimate the maximum recommended detector size a hard cut requiring at least 30 scintillation photons to be detected was implemented. This is a somewhat arbitrary, however it is based on work in [21], where a multi-coincidence trigger applied to the ^{6}LiF:ZnS scintillator

2021 JINST 16 P11039

emission was shown to have maximal efficiency when requiring approximately 10 consecutive single photon trigger stages. A larger but similar order of magnitude cut of at least 30 single photons is deemed reasonable to provide an approximate guide, given that several other inefficiencies are neglected in this work (light guide roughness, coupling inefficiencies, end mirror optimisation). This cut suggests that when using a clear light guide which does not include any wavelength shifting material, the maximum detector length is likely to be 12 cm for a 38 mm photo multiplier tube, with over 75% of the scintillator layer producing very weak scintillation events. When moving to segmented light guides the maximum length is even further reduced to only 5 cm, due to direct photons scattering on the outer surface of the thinner acrylic rods. For all light guide materials considered no significant difference in efficiency is seen for a nine or seven rod configuration.

Light guides with an absorption length and emission spectrum matching EJ280 show a significantly improved light collection efficiency for all geometries that extended to the full 50 cm proposed length of the detector when assuming an absorption length of 3.5 m. Light guides using a segmented central light guide produce an slight increase in light yield over the solid cylindrical detector for normal acrylic (SUVT/UF3) due to an increase in their trapping efficiency when propagating down their full length, however this effect is insignificant when comparing light guide geometries using wavelength shifting materials. When assuming a reduced absorption length of 56 cm the "Fluorescent" light guide geometry still has a significantly improved light collection efficiency compared to the clear acrylic case, despite the shift to a region of lower PMT quantum efficiency. As expected, the BN:ZnS detector simulations show a light yield approximately 50% that of ^{6}LiF:ZnS, highlighting that a maximum detector size of 7 cm is recommended without using wavelength shifting light guides to improve light collection efficiency, whilst detectors approximately 30 cm in length may still be appropriate when utilising low cost fluorescent rods.

These studies suggest that using ^{6}LiF:ZnS foils coupled with low cost fluorescent light guides will result in neutron captures producing events with roughly 30–100 photons within the first 30–50 cm of the detector. In the next section the development of a simple portable detector system for these detectors based on this configuration is discussed.

5 Detector prototypes

Based on the simulations in the previous section a detector prototype was constructed from commercially available fluorescent rods and ^{6}LiF:ZnS scintillator foils. This wrapped light guide geometry was coupled to an ET-Enterprises 9902B PMT, and placed inside a light-tight outer detector housing. The assembled internal light guide geometries and final assembled detector tube are shown in figure 7. An external moderator shield was constructed from a 100 mm outer diameter PVC tube (thickness 1.5 mm) and filled with HDPE beads to give an effective moderator thickness of 30 mm following the LDPE studies described in section 3. Whilst the PVC tubes in the detector act as a thermal neutron absorber, they contribute only 7% of the moderator thickness. Simulations with non-PVC outer tubes were found to show no significant increase in the detector efficiency. Pulses from each detector were digitized using a DRS4 1-GHz digitiser connected to a Raspberry Pi single board computer. The High Voltage (HV) bias value of each PMT was calibrated using a digital to analog convertor connected to the HV base to give an equivalent gain for each PMT. The total power consumption of the PMT, digitiser, and single board computer was found to be less than 4 W. The

2021 JINST 16 P11039

Figure 7. Assembled detector prototype. (left) Bare detector tube before being surrounded in LDPE moderator. (right) Assembled IP55 weatherproof detector system mounted onto a pole.

readout electronics in the (PMT, HV Base, and DRS4) all have an operating range between −40 and 60°C. Similarly the Raspberry Pi has an operating temperature of −40°C to 85°C when operating without LAN active. Installing this system inside an IP55 weatherproof case resulted in a compact and mobile system ready for outdoor use as shown in figure 7.

Neutron pulses were discriminated from background by using software-based pulse shape discrimination. Events were first triggered in hardware on the DRS4 with a trigger threshold of −50 mV, before being transferred to the Raspberry Pi for software processing. A Pulse Shape Discrimination (PSD) metric was calculated from two gated integrals. The "short" integral was defined as the total pulse area below −5 mV and between −5 ns and +25 ns relative to the trigger time. The "long" integral was defined as the total pulse area below −5 mV and between +25 ns and +800 ns. The PSD metric was then defined as the ratio of short/long integrals. The distribution of the PSD metric for different short pulse integrals is shown in figure 8 for a 24 hour exposure when operating the detector outside. A neutron PSD trigger was issued for any short/long ratio greater than 2. The timing windows and PSD trigger threshold were optimised based on initial tests with and without high activity Cf-252 and Cs-137 sources.

Example "neutron" and "background" pulses identified using this PSD metric are shown in figure 8. Lab tests using Cf-252 and Cs-137 sources were performed to assess the ability to detect neutrons using the PSD metric. As shown in figure 8 in the presence of a neutron radiation source an excess of events with a PSD > 2.0 is observed. A small number of high PSD events are observed in the background scenario which are due to a small number of cosmic ray neutron events entering the testing facility. In comparison an excess is seen only at low PSD when the detector is exposed to a gamma ray source. Following an analysis of different pulse shape metrics it was observed that since the dominant detector background was from much shorter pulses, it was also possible to select

2021 JINST 16 P11039

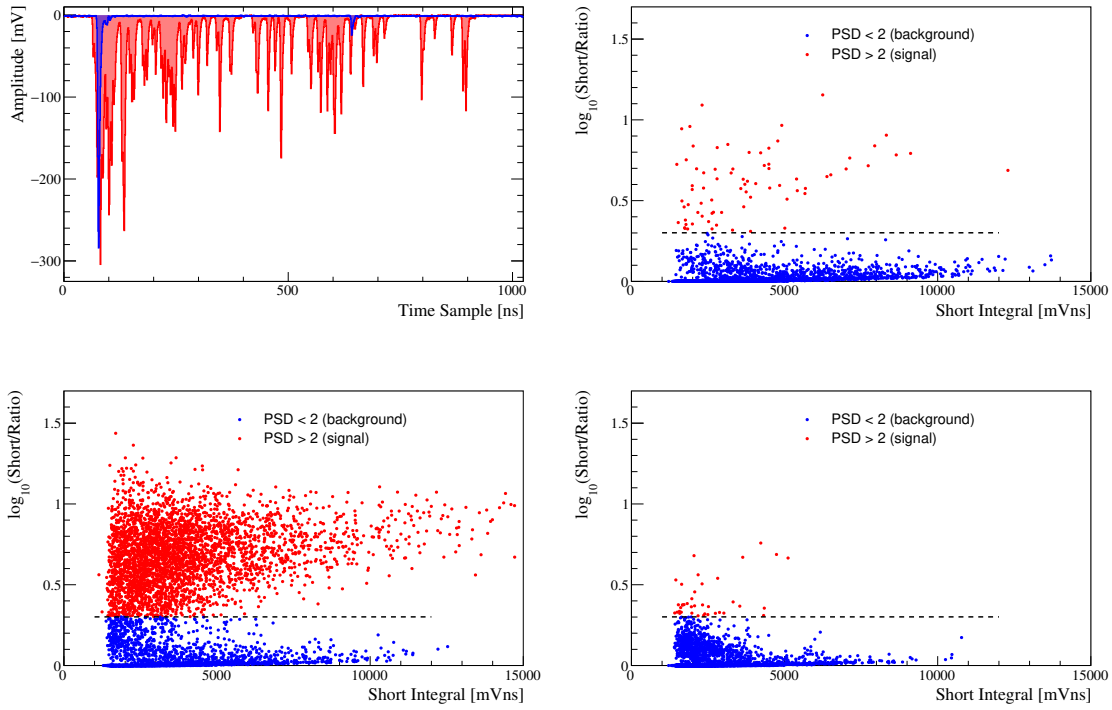

Figure 8. PSD distributions compared between a Cf-252 test source and a background testing case. (Top-left) Example pulse distributions for a gamma [blue] induced and neutron [red] induced event. (Top-right) PSD short/long distribution for backgrounds events. (Bottom-left) Time-over-threshold distribution obtained when the moderated detector was exposed to a Cf-252 source. (Bottom-right) PSD short/long distribution when the moderated detector was exposed to a Cs-137 source.

neutrons in the top region of the PSD plots shown in figure 8 using a simpler Time-Over-Threshold (TOT) cut applied to the digitized data in software. Figure 9 shows the selection of events in each PSD distribution with a TOT $>$ 100 ns. This alternative trigger condition is adopted in all of the software trigger analyses for the rest of this paper as it represents a trigger condition that can be realised with a simple single channel hardware discriminator.

Table 2 shows the total detector hardware triggers for a range of testing configurations. The addition of Cf-252 source produced an excess of over 3477 identified neutron events compared to only 63 observed in the same time period when no source was present. This Cf-252 source was surrounded by a HDPE moderating shield which shifts the outgoing neutron energy into the epithermal and thermal regime. The total neutron counting rate with this Cf-252 HDPE shield was observed to be less than tests without it, however a significant number of neutrons can be moderated by undergoing scattering within the concrete walls surrounding the detector. This increase in the rate is expected due to a combination of this effect and the much higher number of neutrons being emitted from the un-moderated source.

Additional tests with a Cadmium shield wrapped around the detector demonstrate that approximately 19% of the identified neutrons are from thermal neutrons which is consistent with the earlier efficiency simulations. Additional lead shielding suppressed the total trigger rate in the detector but

2021 JINST 16 P11039

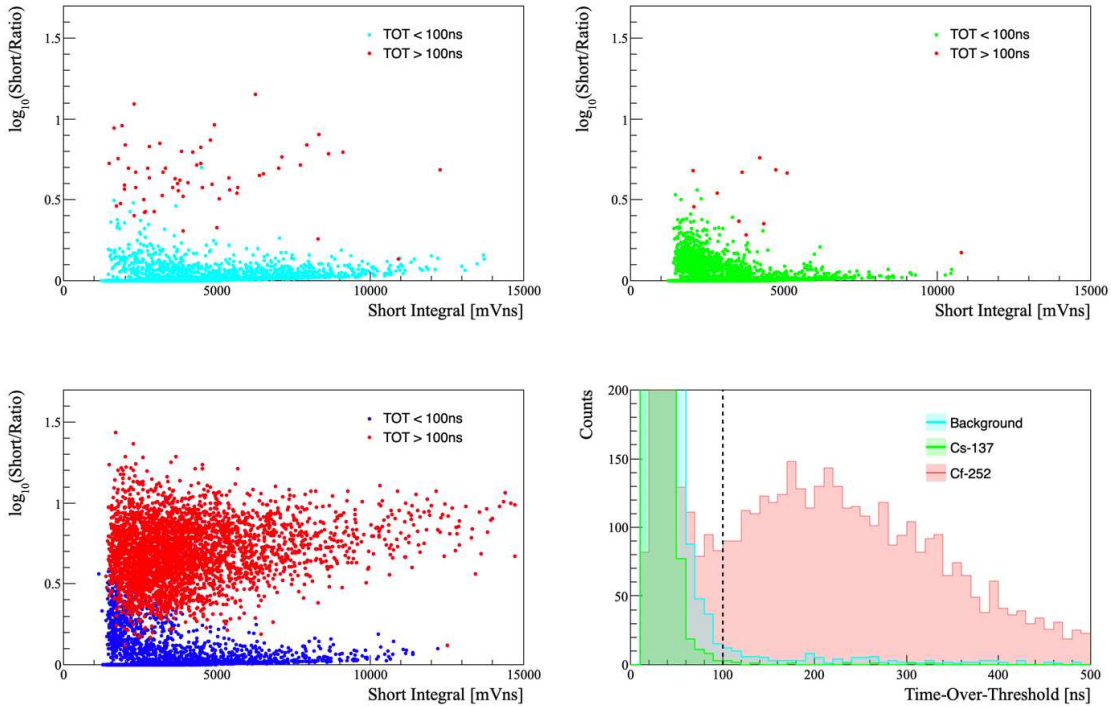

Figure 9. PSD distributions for different testing scenarios. Shown in red in each plot are neutrons identified with a time-over-threshold greater than 100 ns. (Top-left) Background events. (Top-right) Cs-137 gamma events. (Bottom-left) Cf-252 neutron and gamma events. (Bottom-right) Comparison of the TOT for each distribution.

had no observable effect on the total neutron trigger rate. Finally tests with a high activity Cs-137 were found to produce an excess in events in the low TOT regions. Whilst this results demonstrates the scintillating detectors insensitivity to gamma induced events, the drop in the high TOT rate observed with a Cs-137 compared to the background case suggests that the data acquisition system can have a lower neutron triggering efficiency in the presence of a high gamma ray flux due to the deadtime associated with the single threshold hardware trigger. In future work optimisation of a triggering system to select high TOT ^{6}LiF:ZnS pulses entirely in hardware is planned to mitigate this effect. This will result in a lower cost and lower power consumption triggering system suitable for remote cosmic ray monitoring.

6 Online monitoring

To verify that the assembled neutron detector was suitable for the detection of cosmic ray neutrons, long term monitoring data was taken over a period of four weeks with the detector installed outdoors in a residential environment in Durham, U.K. The Raspberry Pi/DRS4 based data acquisition system described in the previous section was extended with a GSM interface hat to allow data to be transferred via 2G to a remote server for further processing. A Luner IoT SIM card was used to provide a network connection, allowing a simple control interface to be built upon Luner's existing IoT communication API, enabling run settings such as high voltage or threshold settings to be

2021 JINST 16 P11039

Table 2. Total detector counts when exposed to a combination of different test sources and shielding setups. HDPE shielding refers to extra moderator shielding surrounding the Cf-252 source itself in addition to the standard LDPE shield on the detector itself. Uncertainties provided are statistical only.

Run	Source	Shield	Total Triggers	20 ns < TOT < 100 ns	TOT > 100 ns
1	Background		2786 ± 52	1275 ± 35	63 ± 7
2	Cf-252	HDPE	6572 ± 81	1523 ± 39	3477 ± 58
3	Cf-252	HDPE + Cd	6092 ± 78	1527 ± 39	2799 ± 52
4	Cf-252	HDPE + Cd + Pb	5400 ± 73	1280 ± 35	2858 ± 53
5	Cf-252	Cd + Pb	7085 ± 84	1188 ± 34	5051 ± 71
6	Cs-137		5174 ± 71	1334 ± 36	11 ± 3

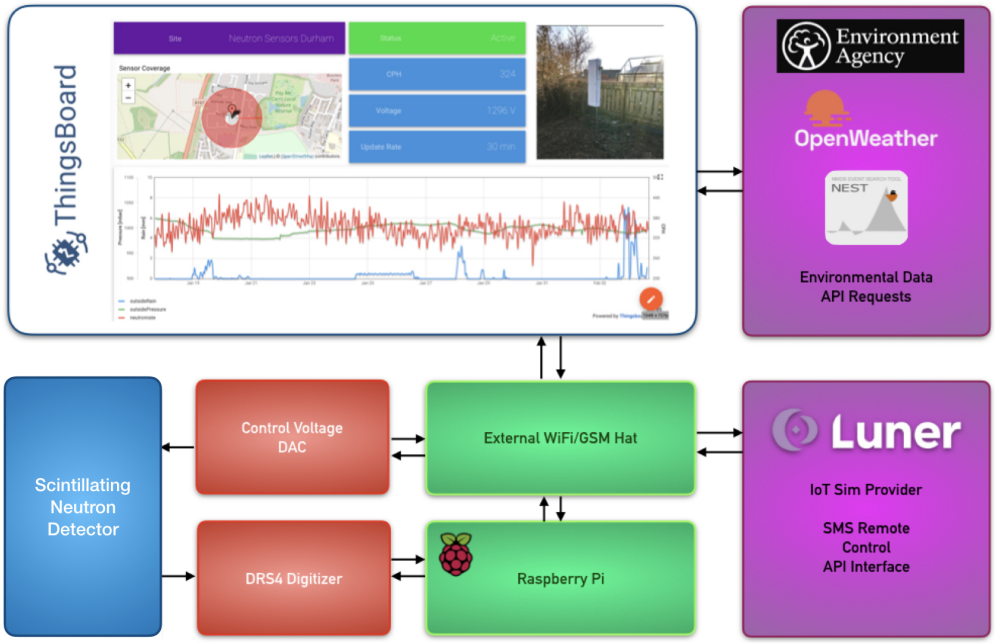

Figure 10. Remote neutron monitoring interface. Data processing is handled server side wherever possible using the open source Thingsboard IoT interface. This allows correlations to be extracted with respect to available weather information for the site, and reduces power consumption by offloading any required data corrections to the remote server.

configured remotely via SMS. Periodic data on local rainfall, pressure, and humidity was obtained automatically via the Thingsboard interface from both the Environment Agency and OpenWeather API. Similarly historic cosmic ray intensity data was obtained at midnight each day from the NEST neutron monitoring database [28] to allow for corrections in the incoming cosmic ray intensity. A diagram of the deployment remote monitoring architecture is shown in figure 10.

Over a period of approximately one month the detector system was found to achieve a good correlation with local pressure variations. As shown in figure 11 these variations were found to agree with the expected exponential drop in the neutron rate with increasing pressure however a small non-varying background rate was observed during the deployment. Modifying the neutron pressure correction function to include an additional non-varying offset term found this additional

2021 JINST 16 P11039

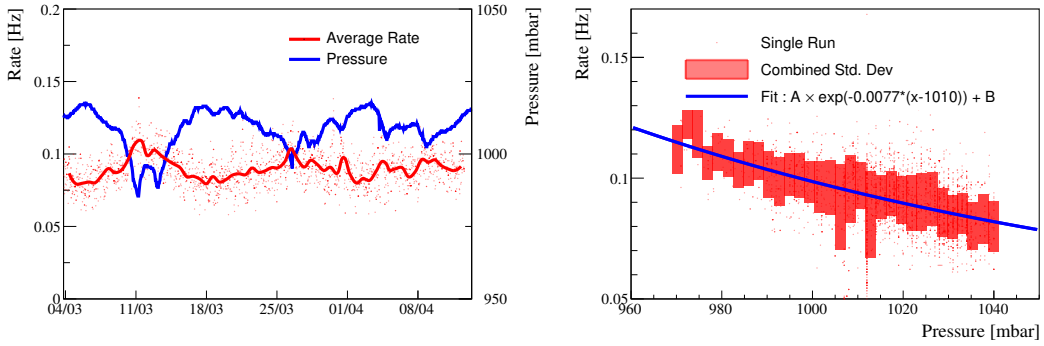

Figure 11. Measured system rate variation over a one month test deployment in a residential area. (left) Measured rate and pressure for each run as a function of date. (right) Correlation between pressure and rate.

contribution to be 0.035 ± 0.011 Hz. Adding extra layers of HDPE shielding at the end of the test period was found to have no effect on this background. This background believed to be due to radon build-up within the scintillator assembly itself over the course of the test deployment. Unfortunately no significant rainfall events occurred during the testing period to investigate whether there was any correlation between event rate increases and environmental release of radon. Work is ongoing to better understand this background and attempt to develop a low power trigger system that can effectively improve the system's signal to noise ratio.

7 Cost analysis

The final trigger rate after the non-varying background was subtracted was found to be approximately 3–4 times lower than expected for a CRS1000 detector. Whilst the use of fluorescent rods with a shorter absorption length limits the maximum length (and therefore counting rate) that a single system can achieve, choosing commercially available off-the-shelf components resulted in a cost saving of around £1200 per detector. This is based on an approximate cost of wavelength shifting PVT sheets of £0.59/cm^2 compared to £0.05/cm^2 for commercial rods. This reduction is comparable to the cost of purchasing an additional photo-multiplier, therefore there is a potential benefit in running multiple scintillating neutron detectors side-by-side to increase the overall system counting rate instead of attempting to extend the system by using longer more expensive light guides.

The scintillator detector system including all supporting peripherals was assembled for approximately £3300, making it applicable for challenges where cost is a higher driving factor compared to temporal resolution. The calculated cost per Counts Per Hour (CPH) of the final detector system came to approximately £9.05/CPH including all supporting power and remote monitoring peripherals. This is significantly less than He-3 based systems (£19.43/CPH), approaching a cost closer to BF3 based systems (£6.10/CPH) [29]. The most expensive components of the tested system are the scintillator foils and the DRS4 digitizer, contributing 21% and 46% of the total detector cost respectively. The adoption of BN based detector foils based on the work shown in section 5 is therefore expected to reduce the overall scintillator cost by a factor of ~ 25 based on estimated manufacturing costs to produce this in-house. In addition the development of lower cost time over threshold discriminators

2021 JINST 16 P11039

is expected to reduce the overall data acquisition cost by a factor of 20. Both of these improvements would result in a BN:ZnS based scintillator system with an expected cost/CPH on the order of £3/CPH.

8 Conclusions and outlook

It has been demonstrated through simulations and field testing that scintillating thermal neutron detectors based upon ^{6}LiF:ZnS scintillator composites are viable solutions for neutron detection in the region of interest for soil moisture monitoring. Simulations of capture efficiency using GEANT4 found no difference in maximum detection efficiency between planar and cylindrical detector geometries when using a fixed volume of scintillator. In addition, simulations of light propagation inside internal light guides showed that wavelength shifting light guides are necessary when assembling cylindrical detectors longer than 5–10 cm. Low cost fluorescent light guides sourced from commercial suppliers were found to have adequate performance when producing smaller detectors approximately 50 cm in length. Extension of the proposed detector geometry beyond 50 cm would likely require custom manufactured rods with an increased absorption length in the 450–500 nm region. Since custom wavelength shifting rods are expected to be significantly more expensive than the commercially available rods considered here, it is still possible that operating multiple 50 cm detectors in parallel could offer a better sensitivity to cost ratio than longer detectors.

The construction and deployment of one of these low-cost 50 cm cylindrical neutron detector system was demonstrated. The system successfully operated without the need for additional fast neutron detectors or expensive PSD-capable digitiser readout electronics. Instead, a simple TOT cut was seen to deliver adequate performance for neutron discrimination at low rates. Based on neutron triggers using a TOT $>$ 100 ns an approximate correlation between neutron counting rate and local pressure data has been demonstrated. This represents a promising first step in the development of low cost thermal neutron scintillator detectors for agricultural applications. In the future it is planned to co-deploy several of these ^{6}LiF:ZnS and BN:ZnS systems alongside an array of commercially available in-ground based soil moisture probes to quantify, with varying choices of thermal neutron shielding materials, both the system performance and the effective detector footprint.

Acknowledgments

P. Stowell would like to thank the Royal Commission for the Exhibition of 1851 for supporting this work. L.F. Thompson and C. Steer would also like to thank the STFC for an earlier Opportunities call which laid the groundwork for this new detector design. P. Stowell would also like to thank P. Chadwick, C. Graham and C. Bourgenot for their guidance and support when measuring emission spectra of light guide geometries.

Conflict of interest. P. Stowell, L. Thompson, and C. Steer are directors of Geoptic Infrastructure Investigations Ltd, a cosmic ray detector company. This work was supported by academic funding steams, and the authors declare that no economic or scientific conflicts of interest may have affected the scientific outputs of this work.

2021 JINST 16 P11039

References

[1] P. Greve, T. Kahil, J. Mochizuki, T. Schinko, Y. Satoh, P. Burek et al., *Global assessment of water challenges under uncertainty in water scarcity projections*, *Nat. Sustain.* **1** (2018) 486.

[2] R. Connor, *The United Nations world water development report 2015: water for a sustainable world*, vol. 1, UNESCO publishing (2015).

[3] M. Zreda, D. Desilets, T.P.A. Ferré and R.L. Scott, *Measuring soil moisture content non-invasively at intermediate spatial scale using cosmic-ray neutrons*, *Geophys. Res. Lett.* **35** (2008) L21402.

[4] M. Köhli, M. Schrön and U. Schmidt, *Response Functions for Detectors in Cosmic Ray Neutron Sensing*, *Nucl. Instrum. Meth. A* **902** (2018) 184 [arXiv:1801.07997].

[5] M. Andreasen, K.H. Jensen, D. Desilets, T.E. Franz, M. Zreda, H.R. Bogena et al., *Status and perspectives on the cosmic-ray neutron method for soil moisture estimation and other environmental science applications*, *Vadose Zone J.* **16** (2017) vzj2017.04.0086.

[6] M. Köhli, M. Schrön, M. Zreda, U. Schmidt, P. Dietrich and S. Zacharias, *Footprint characteristics revised for field-scale soil moisture monitoring with cosmic-ray neutrons*, *Water Resour. Res.* **51** (2015) 5772.

[7] M. Zreda, W.J. Shuttleworth, X. Zeng, C. Zweck, D. Desilets, T. Franz et al., *COSMOS: the COsmic-ray soil moisture observing system*, *Hydrol. Earth Syst. Sci.* **16** (2012) 4079.

[8] J.G. Evans, H.C. Ward, J.R. Blake, E.J. Hewitt, R. Morrison, M. Fry et al., *Soil water content in southern england derived from a cosmic-ray soil moisture observing system — COSMOS — U.K.*, *Hydrolog. Processes* **30** (2016) 4987.

[9] M. Schrön, S. Zacharias, G. Womack, M. Köhli, D. Desilets, S.E. Oswald et al., *Intercomparison of cosmic-ray neutron sensors and water balance monitoring in an urban environment*, *Geosci. Instrum. Meth. Data Syst.* **7** (2018) 83.

[10] M. Andreasen, M. Looms, J.R. Christiansen, T.O. Sonnenborg, S. Stisen and K.H. Jensen, *Examining the canopy interception at a forest field site using cosmic-ray neutron detection*, in *AGU Fall Meeting Abstracts*, vol. 2017, pp. H41D–1481, 2017.

[11] D. Li, M. Schrön, M. Köhli, H. Bogena, J. Weimar, M.A.J. Bello et al., *Can drip irrigation be scheduled with cosmic-ray neutron sensing?*, *Vadose Zone J.* **18** (2019) 190053.

[12] X. Zou, Y. e Li, Q. Gao and Y. Wan, *How water saving irrigation contributes to climate change resilience — a case study of practices in china*, *Mitig. Adapt. Strat. Gl.* **17** (2011) 111.

[13] J. Weimar, M. Köhli, C. Budach and U. Schmidt, *Large-scale boron-lined neutron detection systems as a 3he alternative for cosmic ray neutron sensing*, *Front. Water* **2** (2020) 16.

[14] R.T. Kouzes, A.T. Lintereur and E.R. Siciliano, *Progress in alternative neutron detection to address the helium-3 shortage*, *Nucl. Instrum. Meth. A* **784** (2015) 172.

[15] J.C. Barton, C.J. Hatton and J.E. McMillan, *A novel neutron multiplicity detector using lithium fluoride and zinc sulphide scintillator*, *J. Phys. G* **17** (1991) 1885.

[16] Scintacor product webpage, https://scintacor.com/products/neutron-detection-screens/.

[17] Symetric product webpage, https://symetrica.com/technology/.

[18] L. Stevanato, G. Baroni, Y. Cohen, C.L. Fontana, S. Gatto, M. Lunardon et al., *A novel cosmic-ray neutron sensor for soil moisture estimation over large areas*, *Agriculture* **9** (2019) 202.

2021 JINST 16 P11039

[19] Y. Yehuda-Zada, K. Pritchard, J. Ziegler, C. Cooksey, K. Siebein, M. Jackson et al., *Optimization of 6lif:ZnS(ag) scintillator light yield using GEANT4*, *Nucl. Instrum. Meth. A* **892** (2018) 59.

[20] E.J. Marsden, *Large area thermal neutron detectors for security applications*, Ph.D. thesis, University of Sheffield, Sheffield (2013).

[21] A. Stoykov, J.-B. Mosset and M. Hildebrandt, *Trigger efficiency of a ZnS:6lif scintillation neutron detector readout with a SiPM*, *IEEE Trans. Nucl. Sci.* **63** (2016) 2271.

[22] C. Cowles, S. Behling, P. Baldez, M. Folsom, R. Kouzes, V. Kukharev et al., *Development of a lithium fluoride zinc sulfide based neutron multiplicity counter*, *Nucl. Instrum. Meth. A* **887** (2018) 59.

[23] R.R.S. de Mendonça et al., *The Temperature Effect in Secondary Cosmic Rays (muons) Observed at the Ground: Analysis of the Global Muon Detector Network Data*, *Astrophys. J.* **830** (2016) 88.

[24] A.H. Maghrabi, H. Alharbi, Z.A. Al-Mostafa, M.N. Kordi and S.M. Al-Shehri, *The KACST muon detector and its application to cosmic-ray variations studies*, *Adv. Space Res.* **50** (2012) 700.

[25] M. Abdullrahman, A. Abdulah and A. Mohammed, *First observations of cosmic ray neutrons by a mini neutron monitor at riyadh, saudi arabia*, *Int. J. Astron. Astrophys.* **10** (2020) 319.

[26] GEANT4 collaboration, *GEANT4–a simulation toolkit*, *Nucl. Instrum. Meth. A* **506** (2003) 250.

[27] D. Desilets, M. Zreda and T.P.A. Ferré, *Nature's neutron probe: Land surface hydrology at an elusive scale with cosmic rays*, *Water Resour. Res.* **46** (2010) W11505.

[28] H. Mavromichalaki, A. Papaioannou, C. Plainaki, C. Sarlanis, G. Souvatzoglou, M. Gerontidou et al., *Applications and usage of the real-time neutron monitor database*, *Adv. Space Res.* **47** (2011) 2210.

[29] A. Patrignani, T.E. Ochsner, B. Montag and S. Bellinger, *A novel lithium foil cosmic-ray neutron detector for measuring field-scale soil moisture*, *Front. Water* **3** (2021) 673185.

2021 JINST 16 P11039